

# Lepton-neutron interaction and S-wave low energy parameters

Jaume Carbonell<sup>1</sup> and Tobias Frederico<sup>2</sup>

<sup>1</sup>*Université Paris-Saclay, CNRS/IN2P3, IJCLab, 91405, Orsay, France*

<sup>2</sup>*Instituto Tecnológico de Aeronáutica, 12.228-900 São José dos Campos, Brazil*

(Dated: May 7, 2024)

A lepton-neutron potential in configuration space is obtained. It is based on the Coulomb plus hyperfine interaction Hamiltonian integrated over the neutron charge and magnetic densities. Different parametrisations of the neutron electromagnetic form factors are compared. It is given in the operator form with a central, spin-spin, tensor and spin-orbit terms. The potentials for lowest partial waves states are presented. We compute the lepton-neutron lepton ( $ln$ ) low-energy parameters for the S-waves, estimate the zero-energy cross sections for higher angular momentum states, and point out a possible divergence in the partial wave summation due to the spin-orbit potential.

PACS numbers:

## I. INTRODUCTION

The lepton-neutron ( $ln$ ) interaction is dominated by electromagnetic effects. At the leading order, they are due to the electric interaction between the point-like lepton ( $l$ ) and the neutron ( $n$ ) internal charge distribution, to the magnetic interaction between  $l$  and  $n$  magnetic moments and to the coupling between the  $n$  magnetic moment in the field created by the  $l$  current. They may have different relative signs and strengths depending on the lepton flavour as well as on the quantum number of the  $ln$  system and, despite of its perturbative character, offer a rich variety of non trivial behaviours. A key point in their theoretical estimation is to properly take into account the neutron's internal electromagnetic structure, obtained through the corresponding electric ( $G_E^n$ ) and magnetic ( $G_M^n$ ) form factors.

The lepton-neutron low-energy parameters (LEP) are fundamental quantities which are worth to estimate and measure. Furthermore, they might have several applications in the precision atomic spectroscopy measurements using  $e$ 's and  $\mu$ 's [1], in determining the deuteron [2] and  $\alpha$ -particle charge radius [3], as well as in solid state physics with low energy  $n$  scattering on materials [4–6]. Future experiments based on muonic X-ray spectroscopy are also proposed to significantly improve the charge radii of light nuclei [7] as well as some beyond the standard model investigations related to, still speculative, new bosons (see e.g. [8]).

The aim of the present article is to obtain a  $ln$  potential in configuration space allowing us to compute, within a non-relativistic dynamics, the LEP parameters as well as the corresponding phase shifts and cross sections for the lowest partial waves. It is based on the Hyperfine Hamiltonian integrated over the  $n$  charge and magnetic densities. The potential has four components: a central part due to Coulomb interaction, a spin-spin and a tensor term due to the dipole-dipole magnetic interaction, and spin-orbit term coupling the  $ln$  relative angular momentum,  $L$ , to the  $n$  spin  $s_n$ . This potential is the keystone to evaluate the electronic effects in the low energy neutron scattering in nuclear atomic targets.

Section II is devoted to describe some selected  $n$  electromagnetic form factors used to derive the corresponding charge and magnetic densities in configuration space.

The  $ln$  electromagnetic potential in configuration space is obtained in section III and the main properties of this interaction in the lowest partial wave are discussed.

The numerical results for the  $ln$  low-energy scattering observables are summarised in Section IV, with special emphasis in the (S-wave) low-energy parameters, phase shifts and zero-energy cross sections and the scattering of  $n$  with electrons-bound-to-atoms (Sub. IV A) and a subsection devoted to the zero-energy scattering with higher partial waves (Sub. IV B). Some final remarks conclude this work in section V.

## II. NEUTRON DENSITIES

The  $n$  – charge  $\rho_c^n(\vec{r})$  and magnetization  $\rho_m^n(\vec{r})$  – densities can be obtained by Fourier transforming the corresponding Sachs electric ( $G_E$ ) and magnetic ( $G_M$ ) form factors in the Breit frame [9]:

$$\rho_{c,m}^n(\vec{r}) = \int \frac{d\vec{q}}{(2\pi)^3} G_{E,M}^n(q^2) e^{i\vec{q}\cdot\vec{r}}$$

$$\iff G_{E,M}^n(q^2) = \int d\vec{r} \rho_{c,m}^n(\vec{r}) e^{i\vec{q}\cdot\vec{r}}, \quad (1)$$

where  $t = q^2 = -Q^2$  is the space-like momentum transfer. By expanding the plane wave in the right-hand side of (1)

$$e^{i\vec{q}\cdot\vec{r}} = 1 + i(\vec{q}\cdot\vec{r}) - \frac{1}{2}(\vec{q}\cdot\vec{r})^2 - \frac{i}{6}(\vec{q}\cdot\vec{r})^3 + \frac{1}{24}(\vec{q}\cdot\vec{r})^4 + \dots$$

and integrating over the angular part, one obtains

$$G(q^2) = G(0) - \frac{\langle r^2 \rangle}{6} q^2 + \frac{\langle r^4 \rangle}{120} q^4 + O(q^6). \quad (2)$$

The (even) radial moments  $\langle r_n^{2k} \rangle_{c,m}$  of the  $n$  charge and magnetic distribution can be alternatively obtained as  $k$ -derivatives of the corresponding form factors with respect

to  $q^2$ :

$$\langle r_n^{2k} \rangle_{c,m} = \frac{(-1)^k k!}{(2k+1)!} \left[ \frac{d^k G_{E,M}}{d(q^2)^k} \right]_{q^2=0}, \quad (3)$$

with  $k = 1, 2, \dots$

### A. Charge density

The  $n$ -charge density  $\rho_c^n$  satisfies

$$\int d\vec{r} \rho_c^n(\vec{r}) = 0,$$

and must reproduce the experimental value of the  $n$  mean squared charge radius [10]:

$$\langle r_n^2 \rangle = \int d\vec{r} r^2 \rho_c^n(\vec{r}) = -0.116 \pm 0.002 \text{ fm}^2$$

If we assume for  $G_E^n$  the simple phenomenological form, suggested by Friar [11]

$$G_E^n(q^2) = \beta_n \frac{q^2}{\left(1 + \frac{q^2}{b_n^2}\right)^3}, \quad (4)$$

with parameters  $b_n = 4.27 \text{ fm}^{-1}$  and  $\beta_n = 0.0189 \text{ fm}^2$ , one gets

$$\rho_c^n(\vec{r}) = \frac{(\beta_n b_n^2) b_n^3}{32\pi} (3-x) e^{-x} \quad r = b_n x, \quad (5)$$

and a  $n$  charge mean squared radius  $\langle r_n^2 \rangle = -0.113 \text{ fm}^2$  (in elementary charge units  $e$ ). Despite its simplicity, Friar form factor (4) gives quite accurate results and allows simple analytical expressions. It was also used in [12] for computing the electromagnetic corrections to the nucleon-nucleon (NN) S-wave low-energy parameters and in [13] to compute  $n$ -deuteron scattering observables.

For the sake of completeness, we have also considered the more accurate  $n$  charge densities proposed by Kelly [14]. It has the form

$$G_E^n(q^2) = \frac{A\tau}{1+B\tau} G_D(q^2) \quad \tau = \frac{q^2}{4m_p^2}, \quad (6)$$

where

$$G_D(q^2) = \frac{1}{\left(1 + \frac{q^2}{b^2}\right)^2} \quad (7)$$

is the dipole form,  $b = 4.27 \text{ fm}^{-1}$  [ $b^2 = 0.71(\text{GeV}/c)^2$ ] and the dimensionless parameters  $A = 1.70 \pm 0.04$ ,  $B = 3.30 \pm 0.32$  were adjusted to reproduce the experimental data.

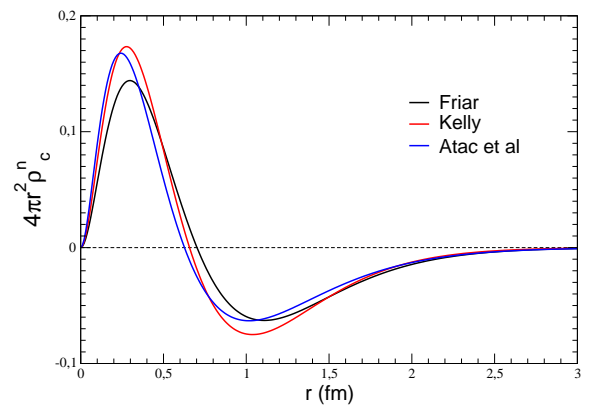
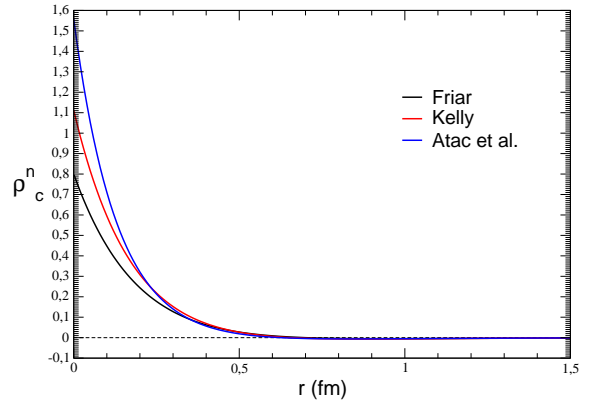


FIG. 1: Neutron charge densities (in elementary charge units  $e$ ):  $\rho_c^n(r)$  (upper panel) and  $4\pi r^2 \rho_c^n(r)$  (lower panel) obtained with different  $n$  charge form factors: Friar (4), Kelly (6) and Atac et al. [15].

The corresponding charge density is

$$\rho_c^n(\vec{r}) = A' \frac{(b\beta)^2}{8(\beta^2 - b^2)^2 \pi} \frac{b^5}{x} \times \left\{ \left[ x + \frac{\beta^2}{b^2} (2-x) \right] e^{-x} - 2 \frac{\beta^2}{b^2} e^{-\beta r} \right\}, \quad (8)$$

with  $A' = \frac{A}{4m_p^2} = 0.01879769 \text{ fm}^2$  and  $\beta = \frac{2m_p}{\sqrt{B}} = 5.234983 \text{ fm}^{-1}$ . It gives a  $n$  charge radius  $\langle r_n^2 \rangle = -0.112 \pm 0.003 \text{ fm}^2$ .

A new parametrisation of the Kelly form factor was recently proposed by Atac et al. [15] with the values  $A = 1.655 \pm 0.126$ ,  $B = 0.909 \pm 0.583$ . This gives  $\langle r_n^2 \rangle = -0.110 \text{ fm}^2$ .

The corresponding  $n$ -charge densities are represented in Fig. 1. Despite reproducing well the experimental  $n$  charge radius, they lead to sizeable different results at small values of  $r$  (factor 2) as well as a 20% difference in the zero of  $\rho_c^n(r)$ .

## B. Magnetic density

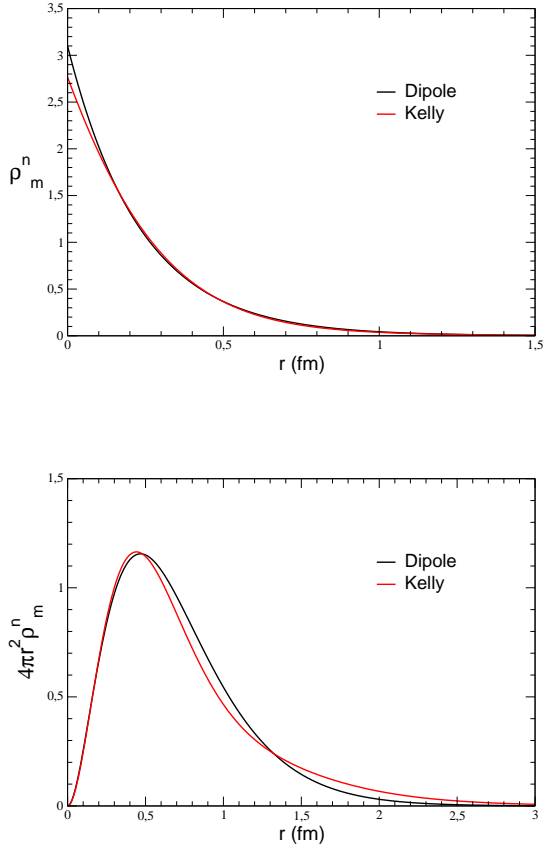


FIG. 2: Neutron magnetic densities (in  $\mu_n$  units):  $\rho_m^n(r)$  (upper panel) and  $4\pi r^2 \rho_m^n(r)$  (lower panel), obtained with different  $n$  magnetic form factors: Dipole (9) and Kelly (11).

The  $n$ -magnetic densities  $\rho_m^n(\vec{r})$  are obtained by Fourier transforming the  $n$ -magnetic form factor  $G_M^n$  and must fulfil

$$\int d\vec{r} \rho_m^n(\vec{r}) = \mu_n,$$

where  $\mu_n$  is the neutron magnetic moment in Bohr magneton units  $\mu_n = -1.91304$ .

By assuming a dipole form for the magnetic form factor [11, 16]

$$G_M^n(q^2) = \frac{\mu_n}{\left(1 + \frac{q^2}{b_n^2}\right)^2}, \quad (9)$$

the  $n$ -magnetic density reads

$$\rho_m^n(\vec{r}) = \mu_n \frac{b_n^3}{8\pi} e^{-x}. \quad (10)$$

We have also considered the more elaborate parametrisation of Kelly, which reads:

$$G_M^n(Q^2) = \mu_n \frac{1 + a_1 \tau}{1 + b_1 \tau + b_2 \tau^2 + b_3 \tau^3}, \quad (11)$$

with  $\tau = \frac{q^2}{4m_n^2}$ , and involve four dimensionless parameters:  $a_1 = 2.33 \pm 1.4$ ,  $b_1 = 14.72 \pm 1.7$ ,  $b_2 = 24.20 \pm 9.8$  and  $b_3 = 84.1 \pm 41$ . The corresponding  $n$ -magnetic densities are depicted in Fig. 2 in  $\mu_n$  units. As one can see, the results for the magnetic density are more stable than for the charge density.

## III. THE LEPTON-NEUTRON INTERACTION

We will consider on the same footing the three elementary leptons ( $e, \mu$  and  $\tau$ ) that will be generically denoted by  $l = e^-, \mu^-, \tau^-$ , as well as their corresponding antiparticles  $\bar{l} = e^+, \mu^+, \tau^+$ . The masses ( $m_l$ ) are taken as  $m_e = 0.510999$  MeV,  $m_\mu = 105.658$  MeV and  $m_\tau = 1776.86$  MeV, and we will assume for all of them a Landé factor  $g_l = 2.00232$  [44], such that their magnetic moments  $M_l$  are given by

$$\begin{aligned} \vec{M}_l &= g_l \frac{q_l \hbar}{2m_l} \vec{S} = \mu_l \vec{\sigma}, \\ \mu_l &= -\frac{g_l}{2} \frac{e\hbar}{2m_l} = -1.00116 \left(\frac{m_e}{m_l}\right) \mu_B, \\ \mu_B &= \frac{e\hbar}{2m_e} = 5.788382 \times 10^{-5} \text{ eV T}^{-1}, \end{aligned} \quad (12)$$

where we denoted  $q_l = -e$ ,  $q_{\bar{l}} = +e$ , and  $e$  is the (positive) elementary charge.

For the neutron we have taken  $m_n = 939.565$  MeV, a Landé factor  $g_n = -3.82608$  and a magnetic moment given by

$$\begin{aligned} \vec{M}_n &= g_n \frac{e\hbar}{2m_p} \vec{S} = \mu_n \vec{\sigma}, \quad \mu_n = \frac{g_n}{2} \frac{e\hbar}{2m_p} = -1.91304 \mu_N, \\ \mu_N &= \frac{e\hbar}{2m_p} = 3.152451 \times 10^{-8} \text{ eV T}^{-1}. \end{aligned} \quad (13)$$

For the remaining constants, we have taken the values  $\hbar c = 197.327$  MeV fm,  $1/\alpha = 137.036$ .

The lepton-neutron ( $ln$ ) interaction is assumed to be purely electromagnetic, which means that we have neglected any weak contribution. The interaction potential we have considered has three components: the Coulomb interaction  $V_{ln}^C$ , the dipole magnetic term  $V_{ln}^{MM}$  resulting from the interaction between the lepton and neutron magnetic moments and the spin-orbit term  $V_{ln}^{LS}$ .

$$V_{ln} = V_{ln}^C + V_{ln}^{MM} + V_{ln}^{LS}. \quad (14)$$

The first term ( $V^C$ ) is the purely Coulomb interaction between the pointlike lepton  $l$  and the  $n$  charge distribution.

The last two terms correspond to the Hyperfine Hamiltonian, as described e.g. in [17, 18], integrated over the magnetization densities. We neglect  $n$  polarization effects which, due to virtual excitations to negative parity states, could lead to a  $1/r^4$  potential with a rich phenomenology of bound and resonant states, like in Refs. [19–22].

Each of the  $V_{ln}$  terms depicted in (14) are detailed in the coming sections.

### A. Coulomb interaction

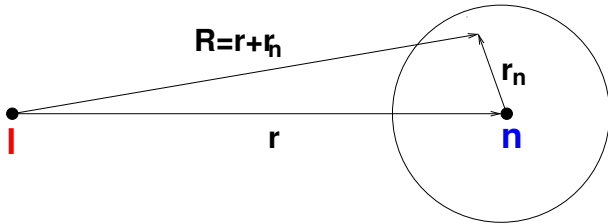


FIG. 3: Interaction between point-like lepton  $l$  and  $n$  charge distribution.

The  $ln$  Coulomb interaction is entirely due to the  $n$  internal structure. It is obtained as a convolution of the Coulomb potential between the point-like lepton with the  $n$  charge density (see Fig. 3):

$$\begin{aligned} V_{ln}^C(r) &= -\frac{1}{4\pi\epsilon_0} \int d\vec{r}_n \frac{e^2 \rho_c^n(\vec{r}_n)}{|\vec{r} + \vec{r}_n|} \\ &= -\alpha(\hbar c) \int d\vec{r}_n \frac{\rho_c^n(\vec{r}_n)}{|\vec{r} + \vec{r}_n|}. \end{aligned} \quad (15)$$

By inserting the Friar electric form factor (4) in the previous expression and making use of

$$\frac{1}{R} = \frac{1}{2\pi^2} \int d\vec{q} \frac{e^{i\vec{q}\cdot\vec{R}}}{q^2},$$

the lepton-neutron Coulomb potential reads:

$$V_{ln}^C(r) = -\alpha(\hbar c) b_n \frac{(\beta_n b_n^2)}{8} (1+x) e^{-x}, \quad x = b_n r. \quad (16)$$

In the point-like limit,  $\beta_n \rightarrow 0$ , and therefore the potential vanishes.

This potential, which is the same for the three leptons, is displayed in the upper panel of Fig. 4 (solid black line) in MeV and fm units. It is monotonously attractive with a depth at the origin of  $V_{ln}^C(0) \equiv C_{ln}^C \approx -0.266$  MeV. We have also included for comparison the results obtained with other parametrisations of the  $n$  charge density represented in the lower panel: the original Kelly parametrisation from [14] (in red) and the recent readjustment of the Kelly parameters from [15] (in blue). Their analytic expressions are quite lengthy and are omitted here. The

noticeable differences observed in the  $n$  charge densities are also manifested in the  $ln$  Coulomb potentials at  $r \approx 0$ .

Notice that for the corresponding antiparticles (in our convention with positive charge), the sign of potential (16) must be changed, giving rise to different  $ln$  and  $\bar{ln}$  low energy parameters. This difference – at first glance surprising since dealing with scattering on a neutral particle – is uniquely due to the neutron’s internal structure.

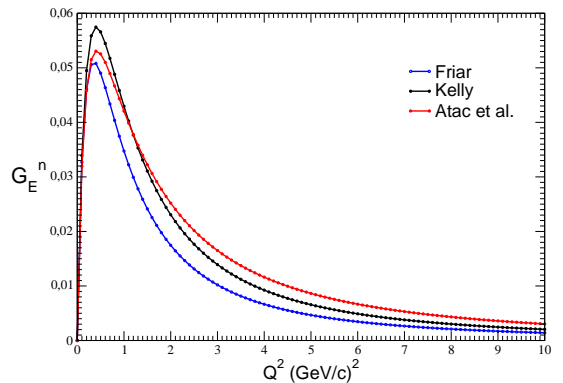
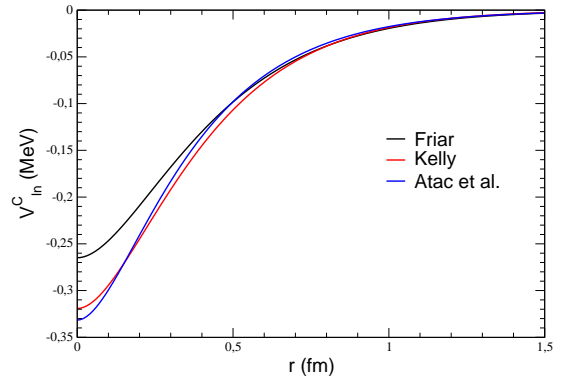


FIG. 4: Upper panel: Coulomb potential between a lepton  $l$  and a neutron  $n$  (in MeV and fm units) with (lower panel) the corresponding  $n$  electric form factors, Friar (4), Kelly (6) and Atac et al. [15], used in their computation. The potential is the same for all leptons.

### B. Magnetic dipole interaction

The interaction between two point-like magnetic moments is given by [17, 18]:

$$\begin{aligned} V_{MM}(\vec{r}) &= -\frac{\mu_0}{4\pi} \left[ \frac{8\pi}{3} \vec{M}_l \cdot \vec{M}_n \delta(\vec{r}) \right. \\ &\quad \left. + \frac{3(\vec{M}_l \cdot \hat{r}_l)(\vec{M}_n \cdot \hat{n}) - \vec{M}_l \cdot \vec{M}_n}{r^3} \right], \end{aligned} \quad (17)$$

which, in terms of (12) and (13), can be written as

$$V_{MM}^{ln}(\vec{r}) = -\frac{\mu_0\mu_l\mu_n}{4\pi} \left[ \frac{8\pi}{3} \vec{\sigma}_l \cdot \vec{\sigma}_n \delta(\vec{r}) + \frac{\hat{S}_{12}(\hat{r})}{r^3} \right], \quad (18)$$

where  $\hat{S}_{12}(\hat{r}) \equiv 3(\vec{\sigma}_1 \cdot \hat{r})(\vec{\sigma}_2 \cdot \hat{r}) - \vec{\sigma}_1 \cdot \vec{\sigma}_2$  is the tensor-operator, whose matrix elements are given by

$$\begin{aligned} \langle SLJ | S_{12} | S' L' J' \rangle &= \delta_{SS'} \delta_{S_1} \delta_{JJ'} \\ &\quad L = J-1 \quad L = J \quad L = J+1 \\ \times \begin{matrix} L = J-1 \\ L = J \\ L = J+1 \end{matrix} &\begin{pmatrix} \frac{-2L}{2L+3} & 0 & \frac{6\sqrt{J(J+1)}}{2J+1} \\ 0 & 2 & 0 \\ \frac{6\sqrt{J(J+1)}}{2J+1} & 0 & \frac{-2(L+1)}{2L-1} \end{pmatrix} \end{aligned} \quad (19)$$

and

$$\langle SLJ | \vec{\sigma}_1 \cdot \vec{\sigma}_2 | S' L' J' \rangle = (-3\delta_{S_0} + \delta_{S_1}) \delta_{SS'} \delta_{LL'} \delta_{JJ'}. \quad (20)$$

In order to take into account the  $n$  magnetization density, the expression for the  $n$  magnetic moment (13) becomes:

$$\vec{M}_n = \mu_n \int \rho_m^n(\vec{r}) \vec{\sigma} d\vec{r}$$

and Eq. (18) is generalized into

$$\begin{aligned} V_{MM}^{ln}(\vec{r}) &= -\frac{\mu_0\mu_l\mu_n}{4\pi} \left[ \frac{8\pi}{3} \vec{\sigma}_l \cdot \vec{\sigma}_n \int d\vec{r}_n \rho_m^n(\vec{r}_n) \delta(\vec{R}) \right. \\ &\quad \left. + \int d\vec{r}_n \frac{3(\vec{\sigma}_l \cdot \hat{R})(\vec{\sigma}_n \cdot \hat{R}) - \vec{\sigma}_l \cdot \vec{\sigma}_n}{R^3} \rho_m^n(\vec{r}_n) \right], \end{aligned} \quad (21)$$

where  $\vec{R} = \vec{r} + \vec{r}_n$ .

By inserting the dipole form factor (9), the integration can be performed analytically, as for the Coulomb case, and the  $ln$  magnetic interaction reads:

$$\begin{aligned} V_{MM}^{ln}(x) &= -\frac{\mu_0\mu_l\mu_n}{4\pi} b_n^3 \left[ \frac{1}{3} e^{-x} (\vec{\sigma} \cdot \vec{\sigma}) \right. \\ &\quad \left. + \frac{1 - \left(1 + x + \frac{x^2}{2} + \frac{x^3}{6}\right) e^{-x}}{x^3} \hat{S}_{12} \right], \end{aligned} \quad (22)$$

where  $x = b_n r$ .

By writing explicitly the scalar spin-spin ( $V_S$ ) and tensor ( $V_T$ ) components we can write (22) in the form:

$$V_{MM}^{ln}(x) = V_S(x) (\vec{\sigma} \cdot \vec{\sigma}) + V_T(x) \hat{S}_{12}, \quad (23)$$

where

$$V_S(x) = -\frac{1}{3} C_{MM}^{ln} e^{-x}, \quad (24)$$

$$V_T(x) = -C_{MM}^{ln} \frac{1 - \left(1 + x + \frac{x^2}{2} + \frac{x^3}{6}\right) e^{-x}}{x^3}, \quad (25)$$

and the (positive) numerical pre-factor

$$C_{MM}^{ln} = \mu_0 \frac{\mu_n \mu_l}{4\pi} b_n^3 = -\frac{g_n g_l}{4} \frac{\alpha (b\hbar c)^3}{4(m_n c^2)(m_l c^2)}. \quad (26)$$

For the electron case ( $l = e^-$ ) it takes the value  $C_{MM}^{en} = 4359.4109 \text{ MeV}$ .

Notice that the  $ln$  magnetic potential (23) for different leptons differs from each other only by the value of this pre-factor, which merely scales the respective ( $V_S$ ) and ( $V_T$ ) components. In view of further discussions, it is interesting to take as a reference the  $en$  case and write

$$V_{MM}^{ln}(x) = \left( \frac{m_e}{m_l} \right) V_{MM}^{en}(x). \quad (27)$$

We have displayed in Fig. 5 the spin-spin ( $V_S$ ) and tensor ( $V_T$ ) components of the reference magnetic potential  $V_{MM}^{en}$ . As one can see,  $V_S$  largely dominates at small distance, where it takes values as large as 1.5 GeV; at  $r=0.5 \text{ fm}$  one still has  $V_S \approx 200 \text{ MeV}$ . Due to the finite size structure of  $n$ , both components are finite in all the domain  $[0, +\infty]$  and  $V_T$  has the asymptotic behaviours

$$V_T(x) \underset{x \rightarrow 0}{\approx} -C_{MM}^{ln} \frac{x}{24}, \quad V_T(x) \underset{x \rightarrow \infty}{\approx} -\frac{C_{MM}^{ln}}{x^3}, \quad (28)$$

with a maximum at  $r \approx 0.4 \text{ fm}$ . We have also included in Fig. 5 the  $V_{MM}^{ln}$  potential provided the Kelly magnetic form factor (11). The result is still analytic but the expression is lengthy enough to be omitted in the text. As was the case for the Coulomb interaction  $V_C$ ,  $V_S$  displays some sizeable differences at  $r = 0$  among the models.

Notice that for the  $en$  case, the Coulomb potential (16), displayed in Fig. 4, is totally negligible with respect to the magnetic one (27). However, while the former is independent of the lepton flavour, the latter one scales with the inverse of lepton mass and the situation is reversed in the case of  $\tau$ .

In view of the sizeable values of the spin-spin component  $V_S$ , the question of a possible  $en$  bound state seems, a priori, pertinent and will be examined in the next section. However, the value of  $\hbar^2/(2\mu_{ne}) \approx 38120 \text{ MeV fm}^2$ , driving the repulsive kinetic energy term, lets very little hope for the  $en$  case. At  $r \approx 0.8 \text{ fm}$  the slow-decreasing tensor component starts being dominant and its  $1/r^3$  tail imposes non trivial asymptotic conditions for the scattering solutions in the spin-triplet ( $S=1$ )  $L > 0$  states, for which the standard LEPs are not defined.

### C. Spin-orbit interaction

Our starting point is the spin-orbit term of the Hyperfine interaction for a point-like lepton [17, 18]:

$$H_{LS}^{ln} = \frac{\mu_0}{4\pi} \frac{e}{m_e} \frac{1}{r^3} \mathbf{L} \cdot \vec{M}_n = -\frac{\mu_0}{4\pi} \frac{e\mu_n}{m_e} \vec{\sigma}_n \cdot \frac{(\mathbf{p} \wedge \mathbf{r})}{r^3}. \quad (29)$$

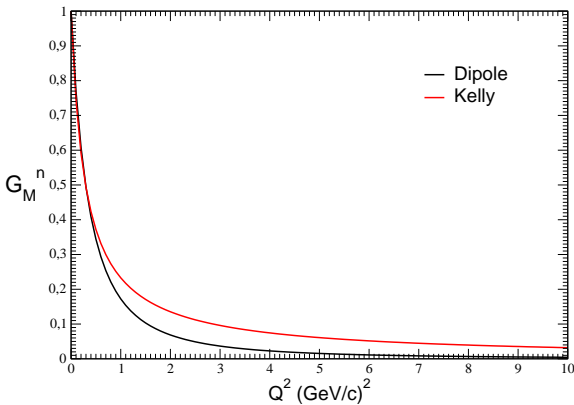
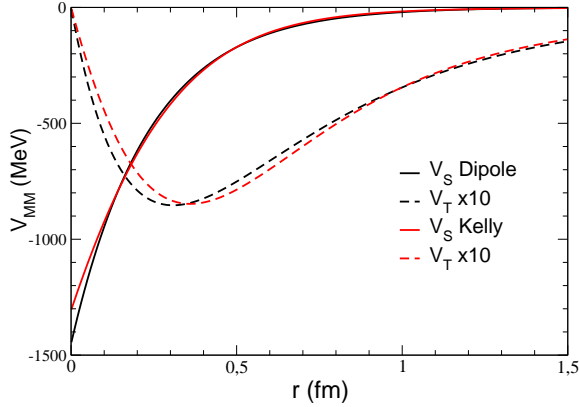


FIG. 5: Upper panel : Spin-spin ( $V_S$ ) and tensor ( $V_T$ ) components of the magnetic interaction (23) between  $e^-$  and  $n$ , corresponding to the Dipole (9) and Kelly (11) magnetic form factors ( $G_M^n$ ), which are represented in the lower panel.

If one takes into account the  $n$  magnetization density, this expression generalizes into

$$H_{LS}^{ln} = -\frac{\mu_0}{4\pi} \frac{e\mu_n}{\mu_{ln}} \vec{\sigma}_n \cdot \mathbf{p} \wedge \int d\mathbf{r}_n \frac{\mathbf{R}\rho_m^n(\mathbf{r}_n)}{R^3}, \quad (30)$$

where we have used the notation of Fig. 3. In principle, an additional term should be added to (30) to account for the coupling between the  $e$  magnetic moment and the magnetic field created by the orbiting  $n$ . The non-zero  $n$  charge density will indeed create a current and the corresponding magnetic field. This term is supposed to be negligible and has been omitted.

By using the same techniques developed for the charge and magnetic terms, one obtains for the spin-orbit interaction the general form

$$V_{LS}^{ln} = V_{LS}(x) (\vec{L} \cdot \vec{s}_n). \quad (31)$$

When inserting the dipole form factor one has

$$V_{LS}(x) = C_{LS}^{ln} \frac{1 - (1 + x + \frac{x^2}{2})e^{-x}}{x^3} \quad (32)$$

with

$$V_{LS}(x) \underset{x \rightarrow 0}{\approx} C_{LS}^{ln} \left[ \frac{1}{6} - \frac{x}{8} + O(x^2) \right], \quad V_{LS}(x) \underset{x \rightarrow \infty}{\approx} \frac{C_{LS}^{ln}}{x^3}, \quad (33)$$

and  $C_{LS}^{ln}$  a (negative, since  $g_n = -3.8261$ ) numerical pre-factor

$$C_{LS}^{ln} = g_n \frac{\alpha(b\hbar c)^3}{(\mu_{ln}c^2)(m_p c^2)}. \quad (34)$$

For the  $en$  case one has  $C_{LS}^{en} = -34853,82$  MeV. The corresponding potential is displayed in Fig. 6. As for the spin-spin term, there is a deep attraction at the origin but it is compensated by the centrifugal barrier in such a way that the effective potential is repulsive everywhere. Remarkably, the reduced spin-orbit potential (i.e.  $v_{LS} = 2\mu_{ln}V_{LS}$ ) is the same for the three leptons.

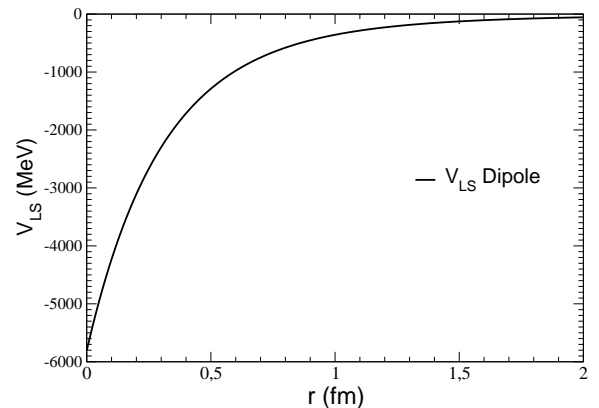


FIG. 6: Spin-orbit potential ( $V_{LS}$ ) for the  $en$  scattering obtained with the Dipole  $n$  magnetic form factor (9).

Notice that the total orbital angular momentum  $L$  of the  $ln$  pair is not coupled to its total spin  $S = s_n + s_e$  but only to the neutron spin  $s_n$ . In this sense, the interaction does not correspond to the standard spin-orbit interaction, although we will keep the same notation to denote it. The main difference is that interaction (31) does not conserve the total spin  $S$  in a similar way that the tensor term does not conserve  $L$ . The matrix elements of the spin-orbit operator (31) in the standard partial wave basis  $|SLJ\rangle$  are:

- Null for S-waves

$$\langle {}^1S_0 | \vec{L} \cdot \vec{s}_n | {}^1S_0 \rangle = \langle {}^3S_1 | \vec{L} \cdot \vec{s}_n | {}^3S_1 \rangle = 0 \quad (35)$$

- For  $L > 0$  triplet unnatural parity states

$$\langle {}^3L_{L\pm 1} | \vec{L} \cdot \vec{s}_n | {}^3L_{L\pm 1} \rangle = \lambda_{\pm}(L) \quad (36)$$

with  $\lambda_{\pm}$  given in (A3).

- They couple the  $L > 0$  singlet and triplet natural parity states

$$\begin{aligned} \langle {}^{2S+1}L_{J=L} | \vec{L} \cdot \vec{s}_n | {}^{2S'+1}L_{J=L} \rangle = \\ = \begin{matrix} S=0 & S=1 \\ S=0 & \begin{pmatrix} 0 & \sqrt{L(L+1)} \\ \sqrt{L(L+1)} & -1 \end{pmatrix} \\ S=1 & \end{matrix} \end{aligned} \quad (37)$$

Their computation requires some care and it is detailed in the Appendix A

#### IV. RESULTS

We present in this Section the scattering results obtained with the above detailed  $V^{ln}$  potentials, for some selected  $ln$  states. To this aim, we write the total potential in the operator form

$$\begin{aligned} V^{ln}(r) = V_C^{ln}(r) + V_S^{ln}(r) (\vec{\sigma}_l \cdot \vec{\sigma}_n) \\ + V_T^{ln}(r) \hat{S}_{12} + V_{LS}^{ln}(r) (\vec{L} \cdot \vec{s}_n). \end{aligned} \quad (38)$$

It depends on four scalar functions  $V_{i=C,S,T,LS}^{ln}$  which change their sign for the antilepton scattering:  $V_i^{\bar{l}n} = -V_i^{ln}$ .

Due to the tensor and spin-orbit terms, the physical states are in general labeled only by  $J^{\pi} = 0^{\pm}, 1^{\pm}, 2^{\pm} \dots$  quantum numbers with  $\pi = (-)^L$ . Calculation are performed in the  $|SLJ\rangle$  basis and we will use the spectroscopic notation  ${}^{2S+1}L_J$  for the tensor and spin-orbit uncoupled states, the standard notation  ${}^{2S+1}L_J - {}^{2S+1}(L+2)_J$  for the tensor coupled ones, and the  ${}^1L_L - {}^3L_L$  for the spin-orbit coupled states.

The matrix elements of the spin-spin, tensor and spin-orbit operators in this basis are given in Table I for the lowest partial waves and the corresponding  $V^{ln}$  potentials are displayed in Fig. 7 for the three considered leptons (in MeV and fm units). Notice the different energy scales among them, varying from few MeV (for  $\tau n$ ) to few GeV (for  $en$ ), which are essentially due to the involved magnetic moments. The  $V^{ln}$  potential is the same for all the singlet states ( ${}^1S_0, {}^1P_1, {}^1D_2, \dots$ ), since the tensor and the diagonal term of  $(\vec{L} \cdot \vec{s}_n)$  vanishes. All potentials are strongly repulsive, except the  ${}^3L_{J=L+1}$  states ( ${}^3S_1$  and  ${}^3P_2$  in the selected ensemble) which are attractive, in absence of the centrifugal term. Let us remind that the situation is however reversed for the antilepton-neutron cases. Notice that for  $en$  case, there is a merging of  ${}^1S_0$ ,  ${}^3P_0$  and  ${}^3P_1$  potentials at  $r=0$ , and that the  ${}^1S_0$  result is getting away when going to  $\mu n$  and  $\tau n$ . The reason for

$J^{\pi}$	${}^{2S+1}L_J$	$\sigma_l \cdot \sigma_n$	$S_{12}$		$\vec{L} \cdot \vec{s}_n$		
		S	S'	L	L'	S	S'
$0^+$	${}^1S_0$	-3		0		0	
$1^+$	${}^3S_1 - {}^3D_1$	+1		0	$2\sqrt{2}$	0	0
				$2\sqrt{2}$	-2	0	-3/2
$0^-$	${}^3P_0$	+1		-4		-1	
$1^-$	${}^1P_1 - {}^3P_1$	-3	0	0		0	$\sqrt{2}$
		0	1		2	$\sqrt{2}$	-1
$2^-$	${}^3P_2 - {}^3F_2$	+1		-2/5	$6\sqrt{6}/5$	+1/2	0
				$6\sqrt{6}/5$	-8/5	0	-2

TABLE I: Angular matrix elements of the spin-spin (20), tensor (19) and spin-orbit (37) operators for the lowest partial waves.

that lies in the particular expressions of potentials and the angular matrix elements presented in Table I. The expressions for these potentials are given below:

$$V_{1S_0}^{ln} = V_C^{ln} - 3V_S^{ln}, \quad (39)$$

$$V_{3P_0}^{ln} = V_C^{ln} + V_S^{ln} - 4V_T^{ln} - V_{LS}^{ln}, \quad (40)$$

$$V_{3P_1}^{ln} = V_C^{ln} + V_S^{ln} + 2V_T^{ln} - V_{LS}^{ln}. \quad (41)$$

At  $r=0$ ,  $V_T$  vanishes and  $V_{3P_0}^{ln}(0) = V_{3P_1}^{ln}(0)$  for all leptons. For the  $en$  case, the equality between these three potentials at the origin is due to the approximate relation  $8C_{MM}^{en} \approx C_{LS}^{en}$  (at the level of 0.1%) that follows from Eqs. (26) and (34) with  $\mu_{en} \approx m_e$  and  $g_e \approx 2$ . This approximate relation is broken when the lepton mass increases from  $e$  to  $\mu$ , and  $\tau$  as clearly seen in the figure.

These potentials are inserted in the set of coupled reduced radial Schrodinger equations

$$\partial_r^2 \varphi_{\alpha}(r) + \left[ k^2 - \frac{L_{\alpha}(L_{\alpha} + 1)}{r^2} \right] \varphi_{\alpha}(r) = \sum_{\beta} v_{\alpha\beta} \varphi_{\beta},$$

where  $v_{\alpha\beta} = \frac{2\mu_{ln}}{\hbar^2} V_{\alpha\beta}(r)$  is the reduced potential and  $k^2 = \frac{2\mu_{ln}}{\hbar^2} E$  is the center of mass momentum. Remarkably, the huge variations observed in Fig. 7 between the different leptons are largely compensated by their reduced mass in  $v_{\alpha\beta}$  and, the resulting  $ln$  scattering observables turn to be quite similar among them, especially in the zero energy limit. This will be presented in the following subsections.

It is worth noticing that, except from the  ${}^1S_0$  and  ${}^3S_1$  states, all the partial waves potentials behave asymptotically as  $1/r^3$ , due to both the tensor and the spin-orbit terms. In this case, the standard scattering theory does not apply [23–29], in particular the low-energy parameters are not defined and the low-energy limit of the cross sections is strongly modified. For the singlet states both terms are absent but, as we have discussed in the previous section, they are coupled by a long-range term to the triplet state, which are driven by the same long-range potentials.

We will present in the next subsection the results for these particular S-waves and devote the last one to de-

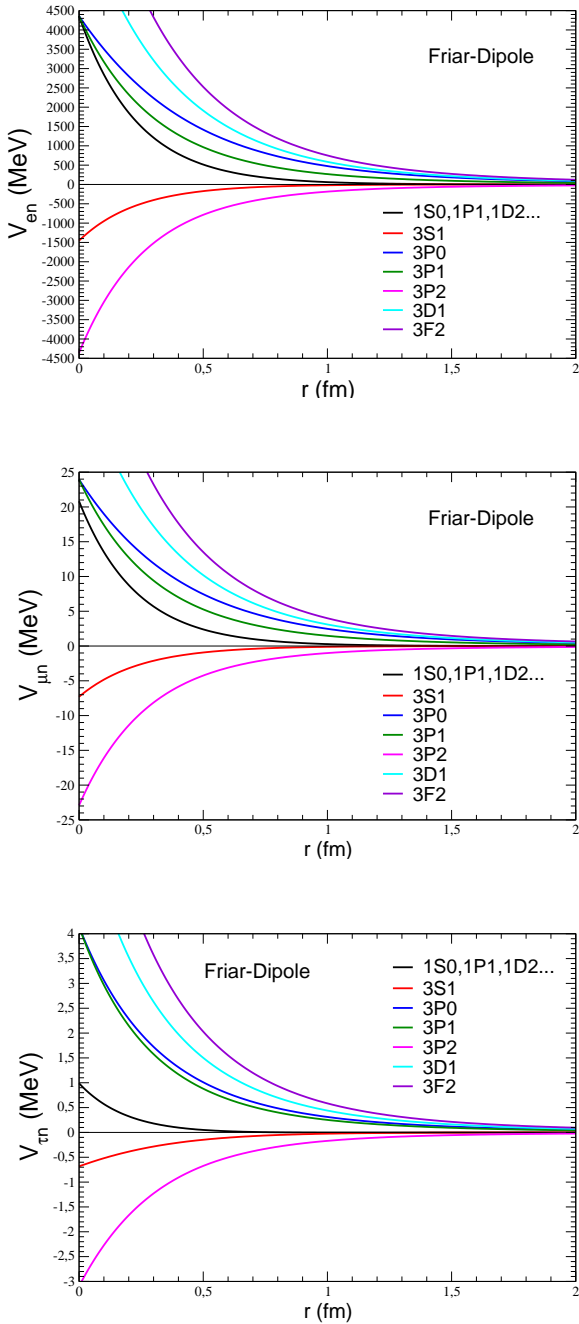


FIG. 7:  $ln$  potentials in different partial waves, obtained with the Friar (electric) and Dipole (magnetic)  $n$  form factors. From top to bottom:  $en$ ,  $\mu n$  and  $\tau n$ .

scribe some low-energy properties of higher angular momentum states.

## A. Low energy parameters for S-waves

We will start with the coherent and incoherent LEPs for the  $^1S_0$  and  $^3SD_1$  states, for which they are well defined. They will be completed by the low-energy phase shifts and cross sections and compared to some experimental results obtained in the low energy  $n$  scattering on atomic systems.

### 1. $^1S_0$

For the S-wave singlet state ( $^1S_0$ ) one has  $\vec{\sigma}_l \cdot \vec{\sigma}_n = -3$ ,  $\hat{S}_{12} = 0$  and  $\vec{L} \cdot \vec{s}_n = 0$ . The  $ln$  potential is given in (39) As seen in Fig. 7, this potential is globally repulsive for all leptons and attractive for antileptons.

The corresponding LEPs are given in Table II in fm units. The different columns correspond to different choices of  $G_E$  and  $G_M$ : Friar (4)+Dipole(9), Kelly(6)+Kelly(11) and Atac[15]+Kelly combination of form factors. The upper half part of the table corresponds to lepton-neutron ( $ln$ ) and the lower part to antilepton-neutron ( $\bar{l}n$ ). Several comments are in order:

- For  $e$  and  $\tau$  there is a nice stability in the predictions for the scattering length among the different  $n$  form factor parametrisations. This is due to the fact that this quantity is essentially dominated by  $V_S$ , which is very similar in the three parametrisations. For the  $\tau$  lepton, the two components of the potential,  $V_C$  and  $V_S$ , become comparable and the scattering length is sensitive to small differences in the  $n$  charge and magnetic form factors.

The effective ranges, on the contrary, show clear discrepancies varying from 20% in the  $en$  and  $\tau n$  cases to more than a factor 10 in  $\tau n$  (including sign).

- For the  $en$  case, the potential is dominated by  $V_S$ , whose contribution, affected by a factor -3, is strongly repulsive ( $\sim 5$  GeV). However when the lepton mass increases, the repulsive  $V_S$  term decreases (as  $m_e/\mu_l$ ) and can be compensated by the attractive  $V_C$ . This is manifested by the decreasing value of the, still repulsive, scattering length  $a_{ln}$  in the upper part of Table II, which in the  $\tau$  case is close to zero. By artificially increasing the lepton mass,  $a_0$  will become negative at  $m_l \approx 1.18 m_\tau$ .
- If the problem was fully perturbative, that is  $T = V$  (where T is the T-matrix obeying the Lipmann-Schwinger equation), one should have  $a_0(ln) + a_0(\bar{l}n) = 0$ . As one can see from Table II by comparing the upper and lower half parts, this condition is quite accurately fulfilled, for  $a_0$  as well as for  $r_0$ . In fact, the value  $s = a_0(ln) + a_0(\bar{l}n)$  constitutes a measurement of the non-perturbative



$^1S_0$	Friar+ Dipole		Kelly+ Kelly		Atac+ Kelly	
	$a_0$	$r_0$	$a_0$	$r_0$	$a_0$	$r_0$
$e^-n$	$2.926 \cdot 10^{-3}$	-149	$2.920 \cdot 10^{-3}$	-186	$2.920 \cdot 10^{-3}$	-186
$\mu^-n$	$2.501 \cdot 10^{-3}$	-170	$2.497 \cdot 10^{-3}$	-215	$2.501 \cdot 10^{-3}$	-215
$\tau^-n$	$1.574 \cdot 10^{-4}$	4814	$1.623 \cdot 10^{-4}$	-2145	$1.849 \cdot 10^{-4}$	-276
$e^+n$	$-2.949 \cdot 10^{-3}$	150	$-2.943 \cdot 10^{-3}$	186	$-2.943 \cdot 10^{-3}$	186
$\mu^+n$	$-2.518 \cdot 10^{-3}$	171	$-2.514 \cdot 10^{-3}$	217	$-2.517 \cdot 10^{-3}$	216
$\tau^+n$	$-1.577 \cdot 10^{-4}$	-4802	$-1.625 \cdot 10^{-4}$	2142	$-1.851 \cdot 10^{-4}$	276

TABLE II: Low energy  $ln$  parameters (in fm) in the  $^1S_0$  state obtained with different choices for the electric (first name heading each column) and magnetic (second name)  $n$  form factors: Friar (4), Dipole (9), Kelly (6) and Atac et al. [15] used to compute the potential.

effects, mainly due to two-photon exchange contributions:

$$T^{ln} + T^{\bar{l}n} = [V + VG_0V + \dots] \\ + [(-V) + (-V)G_0(-V) + \dots] = 2VG_0V + \dots$$

For the  $e$  and  $\mu$ ,  $s \approx 2 \cdot 10^{-5}$  fm, that is about 1%, and for  $\tau$  one order of magnitude smaller.

- In the limit of an infinitely heavy lepton, the potential is given by the Coulomb term and the reduced mass  $\mu_{ln} = m_n$ .
- The most favorable situation to obtain a  $ln$  bound state concerns this channel, not for the  $en$  case since it is repulsive, but for the positron  $e^+n$  and antimuon cases for which  $a \approx -3 \cdot 10^{-3}$  fm. However, the very small values of these scattering lengths tell us that these systems are still very far from a possible bound state. Its very existence would require changing the sign of  $a_0$  after crossing a singularity. It can have some interest to see how far we are from an eventual binding and give no place for eventual further speculations [30–33]. To this aim we have introduced an enhancement factor  $\eta$  in front of the  $V_{1S_0}^{ln}$  potential and determined the critical value of  $\eta$  where  $a_0 \rightarrow +\infty$ , indicating that a zero-energy bound state starts to appear. The result is  $\eta_c = 231$  for  $e^+n$  and  $\eta_c = 266$  for  $\mu^+n$ , far beyond any reasonable uncertainty in the constructed potential.

## 2. $^3S_1$ - $^3D_1$

The  $^3S_1$ - $^3D_1$  state is a coupled channel with the potential matrix

$$V_{^3S_1-^3D_1}^{ln} = \begin{pmatrix} V_C + V_S & 2\sqrt{2}V_T \\ 2\sqrt{2}V_T & V_C + V_S - 2V_T - \frac{3}{2}V_{LS} \end{pmatrix}.$$

However, for this particular state, the diagonal tensor term is zero in the  $^3S_1$  channel and the coupling to the  $^3D_1$  channel is small, as it can be seen from Fig. 5. As a very good approximation we will first consider the  $^3S_1$  channel alone:

$$V_{^3S_1}^{ln}(x) = V_C(x) + V_S(x),$$

in which both components are attractive, giving rise to the unique  $ln$  attractive channel, as seen in Fig. 7. The corresponding LEP parameters are displayed in Table III for the same combinations of  $n$  form factors as in Table II.

When compared to the  $^1S_0$  state one first remarks a much higher stability in the predictions of different form factors, including the  $\tau$  lepton and the effective range parameter  $r_0$ . This is due to the absence of any compensation between the Coulomb ( $V_C$ ) and magnetic ( $V_S$ ) terms, which are both attractive.

One can remark also a kind of flavour independence of the  $ln$  scattering lengths: they vary about 20% while the lepton masses vary over three orders of magnitude. This is the combined consequence of, on one hand, a purely attractive channel (no cancellations between  $V_C$  and  $V_S$ ) and on the other hand, the fact that the reduced spin-spin potential scales as:

$$v_S \equiv \frac{2\mu}{\hbar^2} V_S \sim \frac{m_l m_n}{m_l + m_n} \frac{1}{m_l m_n} \sim \frac{1}{m_l + m_n}. \quad (42)$$

For the  $en$  and  $\mu n$  systems,  $v_S$  is the dominant contribution of the total potential  $v^{ln}$ , while for  $\tau n$ ,  $v_S$  is suppressed by a factor of  $\sim m_n/(m_\tau + m_n) \approx 1/2$  with respect to  $en$  and  $\mu n$  and becomes comparable and even smaller than the reduced Coulomb potential  $v_C$ . The final reduced potential  $v = v_C + v_S$ , in the region of interest to determine the scattering length,

$$a_0^B = \int_0^\infty dr r^2 v(r) \quad (43)$$

turns to be roughly independent of the lepton mass. We have illustrated this fact by plotting in Fig. 8 the integrand of eq. (43) for the different leptons as well as the purely Coulomb potential.

Notice also that the non-perturbative effects are one order of magnitude smaller than for  $^1S_0$ , with  $s \approx 10^{-6}$  fm for  $e$  and  $\mu$ . The coupling to the  $^3D_1$  channel by the small tensor force  $V_T$  does not modify sizeably the value of the  $^3S_1$  scattering lengths given in Table III.

Concerning the possibility of an eventual bound  $en$  state in this channel, the critical enhancement factor – defined in the previous subsection – is  $\eta_c = 690$  for  $en$ ,

${}^3S_1$	Friar+Dipole		Kelly+Kelly		Atac+Kelly	
	$a_0$	$r_0$	$a_0$	$r_0$	$a_0$	$r_0$
$e^-n$	$-0.981 \cdot 10^{-3}$	448	$-0.979 \cdot 10^{-3}$	559	$-0.979 \cdot 10^{-3}$	559
$\mu^-n$	$-1.015 \cdot 10^{-3}$	462	$-1.012 \cdot 10^{-3}$	546	$-1.009 \cdot 10^{-3}$	557
$\tau^-n$	$-1.200 \cdot 10^{-3}$	498	$-1.192 \cdot 10^{-3}$	482	$-1.117 \cdot 10^{-3}$	535
$e^+n$	$0.979 \cdot 10^{-3}$	-448	$0.977 \cdot 10^{-3}$	-559	$0.977 \cdot 10^{-3}$	-559
$\mu^+n$	$1.012 \cdot 10^{-3}$	-461	$1.010 \cdot 10^{-3}$	-545	$1.006 \cdot 10^{-3}$	-556
$\tau^+n$	$1.200 \cdot 10^{-3}$	-497	$1.189 \cdot 10^{-3}$	-481	$1.117 \cdot 10^{-3}$	-535

TABLE III: Low energy  $ln$  parameters (in fm) in the  ${}^3S_1$  state, with the same conventions as in Table. II.

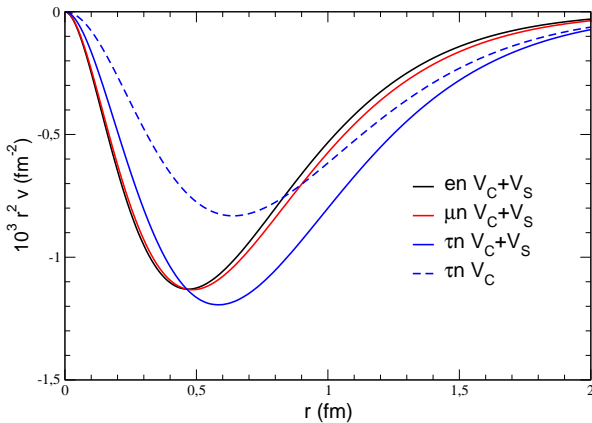


FIG. 8: Reduced  ${}^3S_1$  potentials (42) multiplied by  $r^2$  for the three different  $ln$  systems depicted by solid lines. The dashed line is the reduced Coulomb potential for the  $\tau n$  system.

roughly a factor 3 larger than for  ${}^1S_0$  state, the same factor that exists between the respective potentials.

### 3. $S$ -wave phase shifts, cross sections and coherent scattering lengths

The  $ln$  phase shifts have been computed by solving the Schrödinger equation up to a center of mass energy  $E_{cm}$  half of the  $ln$  reduced mass  $\mu_{ln}$ , i.e. up to center of mass momentum  $k_{max} = \mu_{ln}/\hbar c$ . This defines our kinematical constraint; beyond, a relativistic dynamics would be required. In this kinematical domain, the computed phases are accurately reproduced by the effective range expansion

$$k \cot \delta_0(k) = -\frac{1}{a_0} + \frac{1}{2}r_0 k^2$$

$$\implies \delta_0(k) = -k a_0 \left[ 1 + \frac{1}{2}r_0 a_0 k^2 + \dots \right]. \quad (44)$$

with parameters given in Tables II and III.

They are represented in Fig. 9 as a function of  $E_{cm}$ . As one can see, all phase shifts are very small in the consid-

ered kinematical region. As expected, the perturbative treatment gives accurate result, up to a degree that we have discussed in the previous section.

Obtaining a departure from the linear behaviour at the origin given by  $\delta_0(k) = -k a_0$  in (44), would require  $r_0 a_0 k^2 \sim 1$ . As one can see from Tables II and III, the product  $r_0 a_0$  takes, for both S states and all considered leptons, similar values  $\sim 0.4 - 0.8 \text{ fm}^2$ . Thus, the effective range manifests only above  $k \sim 1 \text{ fm}^{-1}$ , which is – between our kinematical constraint – realized only for the  $\tau n$  ( $k_{max}=3.11 \text{ fm}^{-1}$ ), and to a less extent for  $\mu n$  ( $k_{max}=0.48 \text{ fm}^{-1}$ ). In the  $en$  case the phase shifts are accurately given by  $\delta_0(k) = -a_0 k$ .

The  $ln$  total S-wave cross section takes the form

$$\sigma_{ln}(k) = \frac{1}{4}\sigma_s(k) + \frac{3}{4}\sigma_t(k) \quad \text{with} \quad \sigma_{i=s,t} = 4\pi \frac{\sin^2 \delta_i(k)}{k^2},$$

where the index  $s$  denotes the singlet  ${}^1S_0$  state,  $t$  the triplet  ${}^3S_1$ . The zero-energy limit is given by

$$\sigma_{ln}(0) = \pi(|a_s|^2 + 3|a_t|^2),$$

and provides similar values for the three considered leptons:  $\sigma_{en}(0)=0.358 \mu b$ ,  $\sigma_{\mu n}(0)=0.292 \mu b$ ,  $\sigma_{\tau n}(0)=0.136 \mu b$  [45].

Before concluding this section it is worth considering the  $ln$  coherent scattering length, defined as

$$a_c = \frac{a_s + 3 a_t}{4}. \quad (45)$$

By inserting in (45) the results of Tables II and III, one gets the  $a_c$  values displayed in the upper half part of Table IV (in fm). For the  $en$  and  $\mu n$  cases, there is a remarkable stability with respect the different choices of form factors but for  $\tau n$  they can differ by up to 50%.

Notice that, in the Born approximation, i.e.  $T \equiv V$ , the coherent scattering length (45) would be entirely given by the spin-independent Coulomb potential  $V_C$ . Indeed, in this case the singlet ( ${}^1S_0$ ) and triplet ( ${}^3S_1$ ) contributions to  $a_c$  coming from the spin-spin magnetic term  $V_S$  would exactly compensate each other, due to the  $(\vec{\sigma}_l \cdot \vec{\sigma}_n)$  term, and any non zero value of  $a_c$  would entirely come from  $V_C$ .

We can check this fact by switching off the magnetic term  $V_S$  in the potentials and obtain in this way the "pure Coulomb" coherent scattering length, denoted by

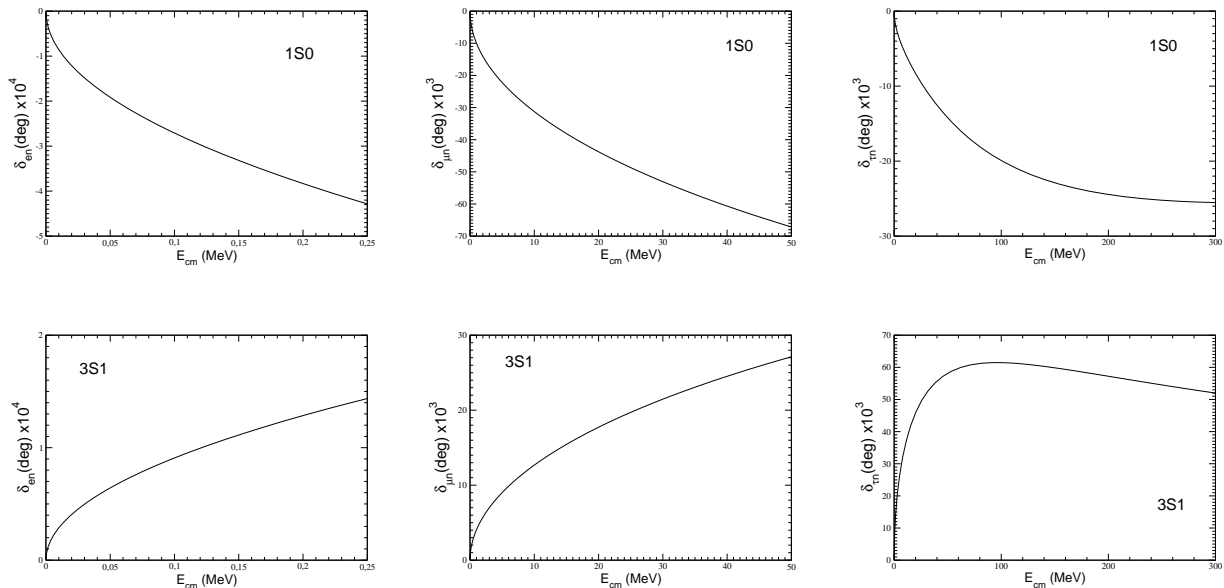


FIG. 9:  $ln$  S-wave phase shifts (in degrees) as a function of cm energy  $E_{cm}$ .

$a_c^C$ . The result is given in the lower half part of Table IV. For the  $\mu n$  case,  $a_c^C$  and  $a_c$  are indeed practically identical, and for  $\tau n$  both quantities are very close. However in the  $en$  case, the value of the coherent scattering length  $a_c$  is one order of magnitude larger than what one could expect from the Coulomb potential alone ( $a_c^C$ ). It follows from that the value of the "in flight"  $en$  coherent scattering length is dominated by, and measures, the non-perturbative effects in the  $en$  scattering process. The dynamical reason for this difference is the huge value of the spin-spin potential in the  $en$  case.

	Friar+Dipole	Kelly+Kelly	Atac+Kelly
	$a_c$	$a_c$	$a_c$
$e^-n$	$-4.50 \cdot 10^{-6}$	$-4.42 \cdot 10^{-6}$	$-4.43 \cdot 10^{-6}$
$\mu^-n$	$-1.36 \cdot 10^{-4}$	$-1.35 \cdot 10^{-4}$	$-1.32 \cdot 10^{-4}$
$\tau^-n$	$-5.07 \cdot 10^{-4}$	$-4.88 \cdot 10^{-4}$	$-3.76 \cdot 10^{-4}$
	$a_c^C$	$a_c^C$	$a_c^C$
$e^-n$	$-7.14 \cdot 10^{-7}$	$-7.08 \cdot 10^{-7}$	$-6.90 \cdot 10^{-7}$
$\mu^-n$	$-1.33 \cdot 10^{-4}$	$-1.32 \cdot 10^{-4}$	$-1.28 \cdot 10^{-4}$
$\tau^-n$	$-8.60 \cdot 10^{-4}$	$-8.53 \cdot 10^{-4}$	$-8.31 \cdot 10^{-4}$
$e^+n$	$7.14 \cdot 10^{-7}$	$7.08 \cdot 10^{-7}$	$6.90 \cdot 10^{-7}$

TABLE IV: Coherent  $ln$  scattering lengths  $a_c$  and the value  $a_c^C$  produced by the Coulomb potential  $V_C$  only (in fm units).

Finally the coherent scattering cross sections, given by

$$\sigma_c = 4\pi \left| \frac{1}{4} [f_s(k) + 3f_t(k)] \right|^2,$$

are represented in Fig. 10 as a function of  $k^2$ . They correspond to Atac+Kelly  $n$  form factors. The zero-energy coherent cross section is  $\sigma_c=0.0023$  nb for  $en$ ,  $\sigma_c=2.2$

nb for  $\mu n$  and  $\sigma_c=79$  nb for  $\tau n$ , that is 3-5 orders of magnitude smaller than the incoherent cross sections ( $1$  nb= $10^{-3}$   $\mu$ b= $10^{-7}$  fm $^2$ ).

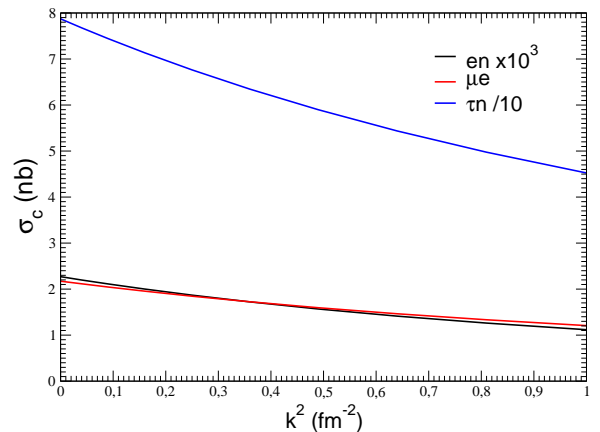


FIG. 10: Coherent  $ln$  scattering cross section (in nb).

To our knowledge, there has been no any measurement of either the coherent or the incoherent  $ln$  cross sections, although it was used in some experiments as a fit parameter for determining the n-"electron-bound-in-a-heavy-atom" coherent scattering length, which is the topic of the next section.

#### 4. $n$ scattering on an "e-bound-to-atom"

A very different situation occurs if one assumes, as was done in the Foldy seminal paper [34] and subsequent reviews on this topic [4, 5], that a very low-energy  $n$  (thermal energies) scatters coherently on a single electron, bound in a heavy atom, which recoils as a whole. In this case the electron can be considered as being infinitely heavy and the reduced mass of the  $ne$  system is equal to the neutron mass:  $\mu_{en} \equiv m_n$ .

One rather talks about the coherent scattering length of a  $n$  colliding with an "electron-bound-to-atom", abusively shortened into  $ne$  coherent scattering length, and traditionally denoted  $b_{ne}$ . In order to distinguish this process from the "on-flight"  $ne$  one described in the previous section, we will use for the former case the notation  $ne^*$  and the corresponding coherent scattering length by  $a_c(ne^*) \equiv b_{ne}$ .

In this approach, the magnetic interaction is disregarded and  $V^{ne^*}$  is simply given by the Coulomb term  $V_C$  - i.e. the  $n$  charge form factor  $G_E$  - which entirely determines the value of  $b_{ne} \equiv a_c(ne^*)$ . [46]

One obtains in this way the  $b_{ne}$  values displayed in Table V, together with the corresponding effective ranges. Notice a three order of magnitude enhancement, of purely kinematical origin, with respect the  $en$  on-line coherent scattering lengths given in Table IV.

The  $b_{ne}$  values presented in Table V are in close agreement with the experimental value  $b_{ne} = -1.32 \pm 0.03$  fm from [6]. It is worth noticing that the value of  $b_{ne}$  - entirely determined by  $G_E$  - is strongly dominated by the the so-called Foldy term [34-37], that is the contribution due to the  $F_2$  Dirac form factor in the standard decomposition of  $G_E$  [38]:

$$G_E(q^2) = F_1(q^2) + \frac{q^2}{4m_p^2} \kappa F_2(q^2).$$

By considering the  $ln$  Coulomb interaction in momentum space

$$V_C \equiv -\frac{\alpha(\hbar c)}{2\pi^2} \frac{G_E(q^2)}{q^2}$$

and applying expansion (2) and (3) to  $G_E$ , one obtains at the lowest order in  $q^2$ , the Born approximation of the  $en$  scattering length displayed in Table V in terms of the moments of the  $n$  radial charge density [5]

$$a_0^B(e^*n) = \frac{(m_n c^2) \alpha}{3(\hbar c)} \langle r^2 \rangle_n, \quad (46)$$

We have shown that the next order in  $q^2$  provides the effective range values

$$r_0^B(e^*n) = -\frac{1}{5 a_0^B(ne^*)} \frac{\langle r^4 \rangle_n}{\langle r^2 \rangle_n}. \quad (47)$$

Due to the perturbative character of the interaction, these relations provide quite accurate results and give some light to the large values of the effective ranges obtained. The former expressions can be generalized to the incoherent LEPS from Tables II and III, provided one properly includes the contribution due to the magnetic form factor  $G_M$ .

Last but not least, we would like to emphasize that, if one takes into account the full magnetic interaction (even a fixed electron keeps its magnetic moment) the results change dramatically. The values of the coherent ( $a_c^*$ ) and incoherent ( $a_{s,t}^*$ ) scattering lengths are given in Table VI for the different choices of  $n$  densities. When compared to the results of Tables II and III one can see a 3 orders of magnitude enhancement due to the kinematical factor. One can remark also a positive sign for the triplet scattering length, whose potential is purely attractive. This indicates the formation of a  $n-e^*$  bound state in this particular channel. Its binding energy is  $B \approx 110$  MeV and the rms radius  $R = \sqrt{\langle r^2 \rangle} = 0.55$  fm. This state corresponds to a pole in the  $n-e^*$  scattering amplitude in the physical energy sheet, although the experimental pertinence of such a result is not clear.

## B. Higher partial waves

All the  $ln$  states with non-zero angular momenta ( $J^\pi = 0^-, 1^-, 2^-, 2^+, 3^-, 3^+, \dots$ ) involve  $|SLJ\rangle$  coupled channels. This coupling is produced by  $1/r^3$  long-range potentials which are due to the tensor ( $V_T$ ) and spin-orbit ( $V_{LS}$ ) terms in (14). Solving the coupled-channel scattering problem with a long-range coupling between channels requires specific methods, like those developed in Refs [39, 40], and it is beyond the scope of the present work.

However one can obtain an estimation of the scattering amplitude and cross section for non-zero angular momentum states by neglecting the coupling among the channels and considering decoupled  $|SLJ\rangle$  states. Still we will be faced with the non trivial problem of scattering by a short-range plus asymptotically  $1/r^3$  potential. It is well known from the early sixties [23-27] that the  $1/r^3$  asymptotic behaviour of the interaction precludes the existence of low-energy parameters.

The simplest case is provided by the spin singlet states, only affected by the short-range  $V_C$  and  $V_S$ , and for which we can compute the LEPS. The results for  ${}^1P_1$  and  ${}^1D_2$  scattering "volumes" are represented in Table VII. One can see very small values of the corresponding scattering volumes with a net decreasing as a function of  $L$ : one order of magnitude each  $L$  ( $10^{-3}$  for  $L=0$ ,  $10^{-4}$  for  $L=1$ ,  $10^{-5}$  for  $L=2$ ). When compared to the S-wave results, one see also a stronger dependence on the choice of  $n$  density parametrizations: a sign inversion for  $\tau$  is present in Friar-Dipole and absent in the other choices, due to the differences in the magnetic form factors. Notice however that these results have only an informative character con-

Friar		Kelly		Atac	
$a_0(ne^*)$	$r_0(ne^*)$	$a_0(ne^*)$	$r_0(ne^*)$	$a_0(ne)$	$r_0(ne^*)$
$-1.32 \cdot 10^{-3}$	501	$-1.31 \cdot 10^{-3}$	449	$-1.27 \cdot 10^{-3}$	518

TABLE V:  $n$ - electron-bound-to-atom ( $ne^*$ ) coherent scattering lengths  $a_0(ne^*) \equiv b_{ne}$  (in fm) produced by  $V_C$  only and with different charge form factors.

	Friar+Dipole	Kelly-Kelly	Atac-Kelly
$a_s^*$	0.843	0.905	0.905
$a_t^*$	0.611	0.567	0.567
$a_c^*$	0.669	0.652	0.652

TABLE VI:  $n$ -electron-bound-to-atom incoherent ( $a_s^*$  and  $a_t^*$ ) and coherent ( $a_c^*$ ) scattering lengths (in fm) produced by the full  $V^{ln}$  interaction.

	Friar+Dipole	Kelly+Kelly	Atac+Kelly
$^1P_1$	$a_1$ (fm <sup>3</sup> )	$a_1$ (fm <sup>3</sup> )	$a_1$ (fm <sup>3</sup> )
$e^-n$	$2.15 \cdot 10^{-4}$	$2.67 \cdot 10^{-4}$	$2.67 \cdot 10^{-4}$
$\mu^-n$	$1.79 \cdot 10^{-4}$	$2.27 \cdot 10^{-4}$	$2.26 \cdot 10^{-4}$
$\tau^-n$	$-2.00 \cdot 10^{-4}$	$0.94 \cdot 10^{-5}$	$0.16 \cdot 10^{-5}$
$^1D_2$	$a_2$ (fm <sup>5</sup> )	$a_2$ (fm <sup>5</sup> )	$a_2$ (fm <sup>5</sup> )
$e^-n$	$1.41 \cdot 10^{-5}$	$3.01 \cdot 10^{-5}$	$3.01 \cdot 10^{-5}$
$\mu^-n$	$1.11 \cdot 10^{-5}$	$2.60 \cdot 10^{-5}$	$2.57 \cdot 10^{-5}$
$\tau^-n$	$-0.34 \cdot 10^{-5}$	$0.39 \cdot 10^{-5}$	$0.18 \cdot 10^{-5}$

TABLE VII: Singlet P- and D-wave  $ln$  scattering "volumes" (the spin-orbit coupling to  $^3P_1$  is neglected).

cerning the short-range part of the interaction, which in its turn produces low-energy partial cross section behaving as  $\sigma_L(k) = |a_L|^2 k^{4L}$ , and so vanishing at  $k = 0$ . Notice also, that the spin-orbit coupling (see Table I) between the singlet states ( $^1L_{J=L}$ ) and the corresponding natural parity triplet states ( $^3L_{J=L}$ ) could dramatically modify the zero energy scattering properties.

For all the other  $L > 0$  states, the  $1/r^3$  behaviour of the interaction prevents a similar study. However, it has been shown in recent works [28, 29] that it is possible to obtain a simple expression for the zero energy cross section, which, contrary to what happens in the case of short-range interactions, does not vanish in the zero energy limit.

The key parameter is the asymptotic coefficient  $\beta_3$  of the (reduced) long range interaction

$$\beta_3 = \frac{2\mu}{\hbar^2} C_3 \quad \text{with} \quad C_3 = \lim_{r \rightarrow \infty} r^3 V(r) \quad (48)$$

It has the dimensions of a length and, in our particular case, it depends on the partial wave  $\beta_3 = \beta_3(L, S, J)$ . Since the central and spin-spin terms in the the  $V^{ln}$  potential are exponentially decreasing,  $\beta_3$  has contributions coming from the tensor and from the spin-orbit potentials. They are obtained by multiplying the asymptotic constants of  $V_T$  (28) and  $V_{LS}$  (33) – which depends on the lepton flavour and on the  $n$  form factor parametrisation – by the corresponding matrix elements of  $S_{12}$  (19)

and  $\vec{L} \cdot \vec{s}_n$  (36)-(37).

It was shown in Refs. [28, 29] that, in the low-energy limit, the PW phase shifts for  $L > 0$  are given by [47]

$$\tan \delta_{L,S,J}(k) = \frac{1}{2L(L+1)} k \beta_3(LSJ) + O(k^2) \quad (49)$$

which entirely depends on the asymptotic coefficient  $\beta_3$  and it is independent of the short-range phase shifts. The scattering amplitude is, in this limit, given by

$$f_{LSJ}(k) = \frac{\tan \delta_L(k)}{k} + O(k) = \frac{\beta_3(LSJ)}{2L(L+1)} + O(k)$$

and the partial cross section

$$\begin{aligned} \sigma_{LSJ}(k) &= (2J+1)\pi |f_{LSJ}|^2 \\ &= (2J+1) \frac{\pi \beta_3^2}{4L^2(L+1)^2} + O(k). \end{aligned} \quad (50)$$

We displayed in Table VIII the asymptotic coefficients  $\beta_3$  (in fm) and the zero-energy partial cross sections provided by Eq. (50) (in  $\mu\text{b}$ ) for the lowest angular momentum states. They correspond to the Friar+Dipole  $n$  form factors.

Our first remark concerns the asymptotic coefficient  $\beta_3$ . As one can see, the triplet natural parity states ( $^3L_{J=L}$ ) have  $\beta_3$  independent of  $L$ , while for the unnatural parity states  $^3L_{J=L\pm 1}$  states,  $\beta_3$  increases with  $L$ . This  $\beta_3(LS, J=L\pm 1)$  increasing is due to both the tensor and the spin-orbit contributions. The tensor contribution increases with  $L$  but converges to a finite value when  $L \rightarrow \infty$  since the tensor matrix elements  $S_{12} \rightarrow -1$ . However the contribution to  $\beta_3(L, S, J=L\pm 1)$  due to the spin-orbit term increases linearly with  $L$ , due the  $\lambda_{\pm}(L)$  eigenvalues (A3).

Our second remark concerns the non-vanishing zero-energy cross section  $\sigma_L(0)$ . They all decrease with increasing  $L$  but for the lowest value of  $L$  represented in Table VIII, they are comparable to the S-wave partial cross sections described in the previous section and which have typical values of  $0.4 - 0.2 \mu\text{b}$ . This is one of the most striking difference with respect the usual scattering by short-range potentials.

A final remark concern the contribution to the total zero-energy cross section from the triplet  $L > 0$  states, as it follows from Eq. (50), and that will be written for

	$e^+n$		$\mu^+n$		$\tau^+ - n$	
	$\beta_3$	$\sigma_L(0)$	$\beta_3$	$\sigma_L(0)$	$\beta_3$	$\sigma_L(0)$
${}^3P_0$	$1.76 \cdot 10^{-2}$	0.61	$1.70 \cdot 10^{-2}$	0.57	$1.38 \cdot 10^{-2}$	0.37
${}^3P_1$	$0.88 \cdot 10^{-2}$	0.45	$0.91 \cdot 10^{-2}$	0.49	$1.07 \cdot 10^{-2}$	0.68
${}^3P_2$	$-5.28 \cdot 10^{-3}$	0.28	$-5.34 \cdot 10^{-3}$	0.28	$-5.67 \cdot 10^{-3}$	0.32
${}^3D_1$	$2.06 \cdot 10^{-2}$	0.28	$2.03 \cdot 10^{-2}$	0.27	$1.86 \cdot 10^{-2}$	0.23
${}^3D_2$	$0.88 \cdot 10^{-2}$	0.08	$0.91 \cdot 10^{-2}$	0.09	$1.07 \cdot 10^{-3}$	0.12
${}^3D_3$	$-1.09 \cdot 10^{-2}$	0.18	$-1.10 \cdot 10^{-2}$	0.18	$-1.15 \cdot 10^{-3}$	0.20
${}^3F_2$	$2.58 \cdot 10^{-2}$	0.18	$2.56 \cdot 10^{-2}$	0.18	$2.43 \cdot 10^{-2}$	0.16
${}^3F_3$	$0.88 \cdot 10^{-2}$	0.03	$0.91 \cdot 10^{-2}$	0.03	$1.07 \cdot 10^{-2}$	0.04
${}^3F_4$	$-1.66 \cdot 10^{-2}$	0.14	$-1.67 \cdot 10^{-2}$	0.13	$-1.73 \cdot 10^{-2}$	0.15

TABLE VIII: Asymptotic coefficients  $\beta_2$  (48) (in fm) and zero-energy partial cross sections (50) (in  $\mu\text{b}$ ) for the lowest non-zero angular momentum states.

latter convenience in the form.

$$\sigma_T(k) = \sum_{J=0} \sigma_J \quad \text{with}$$

$$\sigma_J = \sigma_{L=J-1,1,J} + \sigma_{L=J,1,J} + \sigma_{L=J+1,1,J}.$$

If  $\beta_3$  would be independent of  $L$ , as it is implicitly assumed in [28, 29], the zero-energy cross section  $\sigma_L(0)$  would decrease asymptotically as  $1/J^3$  for all states  $L = J - 1, J, J + 1$  and one could easily obtain the total low-energy cross section. For instance, for natural parity states ( $L=J$ ) one has

$$\sigma_T(k) = \frac{\pi\beta_3^2}{4} \sum_{J=1}^{\infty} \frac{2J+1}{J^2(J+1)^2} = \frac{\pi\beta_3^2}{4}.$$

This is however not the case in the  $ln$  system. In particular, the contribution to the total cross section due the unnatural parity states, is affected by a quadratic dependence on  $J$  due to  $\beta_3(L = J \pm 1)$  and according to (50) one has

$$\sum_{J=1}^{\infty} \sigma_J(0) \sim \sum_{J=1}^{\infty} \frac{1}{J} \quad (51)$$

which is logarithmically divergent with  $J$ . This fact suggests a non integrability of the total differential cross section, and could be either an intrinsic property of the  $1/r^3$  potentials with spin-orbit force, or a consequence of a too restrictive hypothesis in the derivation of (49). References [28, 29] are indeed based on the Born approximation with the asymptotic  $1/r^3$  potentials. It is not clear that this approximation could apply when the asymptotic coefficient  $\beta_3$  of these potentials is very large, even linearly diverging with  $L/J$ . Work is in progress to clarify this point.

## V. CONCLUDING REMARKS

We have presented a lepton-neutron potential in configuration space based on the Coulomb interaction between the pointlike lepton and the neutron charge density plus the hyperfine Hamiltonian integrated over the

neutron electric and magnetic densities. It is given in the operator form and has a central, spin-spin, tensor and spin-orbit terms, all regulars at the origin and the two latter displaying a long-range  $1/r^3$  tail, precluding the existence of low-energy parameters in non-zero angular momentum states. Several parametrisations of the experimentally measured neutron form factors have been used to check the stability of the predictions.

The S-wave lepton-neutron low-energy parameters – coherent and incoherent scattering length and effective range – have been obtained as well as the corresponding cross section. The coherent scattering of  $n$  with "electrons-bound-to-atoms" has been considered and the predictions of the potential have been found in agreement with the experimentally measured value of the coherent n-atom scattering length  $b_{ne} = 1.23 \pm 0.03$  fm. To our knowledge, and apart from this latter quantity, none of the lepton-neutron low-energy parameters have been already predicted and remain experimentally unknown.

The higher angular momentum states are all coupled in the partial wave  $LSJ$  basis, either by tensor force for the triplets unnatural parity states ( ${}^3L=J-1, J-{}^3L=J+1, J$ ) or by spin-orbit term for the single and triplet natural parity states ( ${}^1L_{J=L}$  and  ${}^3L_{J=L}$ ). By neglecting this coupling, we have estimated the low-energy cross section for the lowest partial waves and pointed out a divergence in the partial wave expansion of the total cross section. The origin of this behaviour lies in the spin-orbit interaction for the triplet unnatural parity states, from the combined effect of its long-range tail and the increasing matrix elements with the angular momentum.

The lepton-neutron potentials presented in this work, which are largely dominated by the magnetic terms (tensor and spin-orbit), can be useful as theoretical inputs in the analysis of the precision atomic spectroscopy data with  $e$ 's and  $\mu$ 's beyond the H case. In particular, to extract the nuclear charge radii taking into account the impact of the neutron electromagnetic structure on the electron-nucleus interaction. It is worth mentioning that, contrary to what happens in H isotopes (proton [41, 42] and deuterium [2]), there is no any significant difference between the  $e$  and  $\mu$  results in the  ${}^4\text{He}$  charge radius [3]. A possible reason for that could be the average of the

lepton-nucleon magnetic effects that take place in the  $\alpha$ -particle but is absent in proton and deuterium.

### Acknowledgments

The authors are indebted to R. Lazauskas, B. Mous-salam, D.R. Phillips and H. Sadjan for the very helpful discussions during the elaboration of this work. J.C. thanks the financial support from FAPESP (Fundação de Amparo à Pesquisa do Estado de São Paulo) grant 2022/10580-3. T. F. thanks the financial support from CNPq (Conselho Nacional de Desenvolvimento Científico e Tecnológico) grant 306834/2022-7, CAPES (Coordenação de Aperfeiçoamento de Pessoal de Nível Superior), Finance Code 001, CAPES/COFECUB grant 88887.370819/2019-00, and FAPESP (grants 2017/05660-0 and 2019/07767-1). This work is a part of the project Instituto Nacional de Ciência e Tecnologia - Física Nuclear e Aplicações Proc. No. 464898/2014-5. We have benefited from the French IN2P3 support to PUMA theory project.

### Appendix A: Matrix elements of spin-orbit term

Let us consider the spin-orbit operator in the form

$$\vec{L} \cdot \vec{s}_n = \frac{1}{2} \left[ j_n(j_n + 1) - L(L + 1) - \frac{3}{4} \right],$$

$$\vec{j}_n = \vec{L} + \vec{s}_n, \quad \vec{J} = \vec{j}_n + \vec{s}_e \quad (\text{A1})$$

It is diagonal in the eigenbasis

$$|L, j_n, J = L, L \pm 1\rangle \equiv$$

$$| [L, s_n = \frac{1}{2}]_{j_n=L \pm \frac{1}{2}}, s_e = \frac{1}{2}; J = j_n \pm \frac{1}{2} = L, L \pm 1 \rangle,$$

the spin-orbit matrix elements are:

$$\langle L, j_n = L \pm \frac{1}{2}, J | \vec{L} \cdot \vec{s}_n | L, j'_n = L \pm \frac{1}{2}, J \rangle = \delta_{j j'} \lambda_{\pm}(L) \quad (\text{A2})$$

for  $\forall J = L, L \pm 1$ , with eigenvalues given by the right-hand side of (A1):

$$\lambda_{\pm}(L) = \begin{cases} \frac{L}{2} & \text{if } j_n = L + \frac{1}{2} \\ -\frac{L}{2} - \frac{1}{2} & \text{if } j_n = L - \frac{1}{2} \end{cases} \quad (\text{A3})$$

It is however interesting to know the matrix elements of the spin-orbit operator in the usual partial wave (PW) basis  $|SLJ\rangle$ :

$$\langle SLJ | \vec{L} \cdot \vec{s}_n | S' L J \rangle =$$

$$\sum_{j_n=L \pm 1/2} \langle SLJ | L j_n J \rangle \lambda_{\pm}(L) \langle L j_n J | S' L J \rangle. \quad (\text{A4})$$

The relation between the  $|L, j_n, J\rangle$  and the  $|S, L, J\rangle$  basis is given by the 6j coefficients [43]

$$\langle [(s_e s_n) S L]_J | [s_e (s_n L) j_n] J \rangle =$$

$$(-1)^{J+L+1} \sqrt{(2S+1)(2j_n+1)} \begin{Bmatrix} s_e & s_n & S \\ L & J & j_n \end{Bmatrix}, \quad (\text{A5})$$

with  $s_e = s_n = \frac{1}{2}$ . According to that, most of  $|L, j_n, J\rangle$  states corresponds to a single  $|SLJ\rangle$  state. Thus for S-wave one has :

$$|0, j_n = \frac{1}{2}, J = 0\rangle \equiv |^1 S_0\rangle$$

$$|0, j_n = \frac{1}{2}, J = 1\rangle \equiv |^3 S_1\rangle \quad (\text{A6})$$

and for  $L > 0$  unnatural parity states

$$|L, j_n = L \pm 1/2, J = L \pm 1\rangle \equiv |^3 L_{L \pm 1}\rangle, \quad (\text{A7})$$

where we used the spectroscopic notation

$$|^{2S+1} L_J\rangle \equiv |SLJ\rangle.$$

The corresponding matrix elements of the spin-orbit operator are

$$\langle ^1 S_0 | \vec{L} \cdot \vec{s}_n | ^1 S_0 \rangle = 0 \quad (\text{A8})$$

$$\langle ^3 S_1 | \vec{L} \cdot \vec{s}_n | ^3 S_1 \rangle = 0 \quad (\text{A9})$$

$$\langle ^3 L_{L \pm 1} | \vec{L} \cdot \vec{s}_n | ^3 L_{L \pm 1} \rangle = \lambda_{\pm}(L) \quad (\text{A10})$$

It turns out, however, that the two natural parity states,  $|L, j_n = L \pm \frac{1}{2}, J = L\rangle$ , are (orthogonal) linear combinations of the corresponding singlet and triplet natural parity states, i.e.  $|S = 0, L, J = L\rangle$  and  $|S = 1, L, J = L\rangle$ :

$$\left( \begin{array}{c} |L, j_n = L - \frac{1}{2}, J = L\rangle \\ |L, j_n = L + \frac{1}{2}, J = L\rangle \end{array} \right) = M_L \left( \begin{array}{c} |^1 L_L\rangle \\ |^3 L_L\rangle \end{array} \right),$$

$$M_L = \left( \begin{array}{cc} -\sqrt{\frac{L}{2L+1}} & \sqrt{\frac{L+1}{2L+1}} \\ \sqrt{\frac{L+1}{2L+1}} & \sqrt{\frac{L}{2L+1}} \end{array} \right), \quad (\text{A11})$$

with,  $\det(M_L) = -1$  and  $M_L^{-1} = M_L$ .

The matrix elements of the spin-orbit operator in this basis are obtained by inserting relation (A5) into (A4) and read:

$$\langle ^{2S+1} L_{J=L} | \vec{L} \cdot \vec{s}_n | ^{2S'+1} L_{J=L} \rangle = M_L \begin{pmatrix} \lambda_- & 0 \\ 0 & \lambda_+ \end{pmatrix} M_L, \quad (\text{A12})$$

which leads to Eq. (37). As one can see, the singlet  $|^1 L_J\rangle$  and the triplet  $|^3 L_J\rangle$  states with natural parity (i.e. with  $J=L$ ) are coupled by the spin-orbit term (A1), which generates transitions between them. This is the case for  $^1 P_1 - ^3 P_1, ^1 D_2 - ^3 D_2, ^1 F_3 - ^3 F_3$  etc.

- 
- [1] Nancy Paul, Guojie Bian, Toshiyuki Azuma, Shinji Okada, Paul Indelicato, Phys. Rev. Lett. 126, 173001 (2021)
- [2] R. Pohl, F. Nez, L.M.P. Fernandes et al. Science 353, 669-673 (2016)
- [3] J.J. Krauth, K. Schuhmann, M.A. Ahmed et al. Nature 589, 527-531 (2021).
- [4] V.F. Sears, Phys. Rep. 141 (1986) 281.
- [5] H. Abele, Prog. Part. Nucl. Phys. **60**, 1 (2008)
- [6] L. Koester, W. Waschowski, L. V. Mitsyna, G. S. Samosvat, P. Prokofjevs, J. Tambergs, Phys. Rev. **C51**, 3363 (1995)
- [7] B. Ohayon, A. Abeln, S. Bara et al., Physics 6, 206-215 (2024)
- [8] Menno Door, Chih-Han Yeh, Matthias Heinz et al., arXiv:2403.07792v1 (2024)
- [9] Cedric Lorcé, Phys. Rev. Lett. 125, 232002 (2020)
- [10] R.L. Workman et al. (Particle Data Group), Prog. Theor. Exp. Phys. 2022, 083C01 (2022)
- [11] J.L. Friar and J.W. Negele, Adv. Nucl. Phys. 8, 219 (1975)
- [12] R.B. Wiringa, V.G.J. Stoks and R. Schiavilla, Phys. Rev. 51 (1995) 38
- [13] A. Kievsky, M. Viviani, L.E. Marcucci, Phys. Rev. **C69** 014002 (1004)
- [14] J.J. Kelly, Phys. Rev. **C 70**, 068202 (2004)
- [15] H. Atac, M. Constantinou, Z.-E. Meziani, M. Paolone and N. Sparveris, Nature Comm. 12, 1759 (2021)
- [16] S. Galster et al., Nucl. Phys. **B32** (1971) 221
- [17] J.D. Jackson, Classical Electrodynamics, J. Wiley and Sons, 3rd Ed. (2001)
- [18] J. Mourad, H. Sazdjian, J. Math. Phys. 35 (1994) 6379.
- [19] R. Lazauskas, J. Carbonell, Few-Body Syst 31 (2002)125
- [20] J. Carbonell, R. Lazauskas, D. Delande, L. Hilico, S.Kilic, Europhys Lett 64 (2003) 316
- [21] J. Carbonell, R. Lazauskas, V.I. Korobov, J. Phys. B: At. Mol. Opt. Phys. 37(2004)2997
- [22] Daniel Odell, Daniel R. Phillips and Ubirajara van Kolck, Phys. Rev. **A 108**, 062817 (2023)
- [23] L. Spruch, T. F. O'Malley, and L. Rosenberg, Phys. Rev. Lett. 5, 375 (1960)
- [24] L. Spruch, T. F. O'Malley, and L. Rosenberg,, J. Math. Phys. (N.Y.) 2, 491 (1961)
- [25] E. Del Giudice and E. Galzenati, Il Nuovo Cimento 38, 443 (1965)
- [26] E. Del Giudice and E. Galzenati, Il Nuovo Cimento 40, 739 (1965)
- [27] R. Shakeshaft, J. Phys. B: Atom. Molec. Phys., Vol. 5, June 1972
- [28] Bo Gao, Phys. Rev. **A 59**, 2778 (1999)
- [29] Tim-Oliver Müller, PRL 110, 260401 (2013)
- [30] T.J. Grant and J.W. Cobble, Phys Rev Lett. 23 (1969) 741
- [31] D. W. Schlitt, Phys. Rev. **B 2**, 3437 (1970)
- [32] J.H. McGuire, Am. J. Phys. 40, 617 (1972)
- [33] D.W. Schlitt, Lett. to the Editor, Am. J. Phys. 41, 1120 (1973)
- [34] L.L. Foldy, Review of Modern Physics 30 (1958) 471
- [35] L. Ya. Glozman and D. O. Riska, Phys. Lett. **B459** , 49(1999)
- [36] M. Bawin and S. A. Coon, Phys. Rev. **C60** , 025207-1(1999)
- [37] V.A. Karmanov, Nucl. Phys. **A 699** (2002) 148c
- [38] J.D. Bjorken and S.D. Drell, Relativistic Quantum Mechanics (1964)
- [39] M. Valdes, M. Dufour, R. Lazauskas and P.-A. Hervieux, Phys. Rev. **A 97**, 012709 (2018)
- [40] M. Dufour, M. Valdes, R. Lazauskas and P.-A. Hervieux, Hyperfine Interact (2018) 239: 41
- [41] R. Pohl, A. Antognini, F. Nez et al. Nature 466, 213-216 (2010).
- [42] A. Antognini, F. Hagelstein and V. Pascalutsa, Ann. Rev. Nucl. Part. Sci. 72 (2022) 389
- [43] A. Messiah, Quantum Mechanics, Volume II
- [44] The  $g_l$  values for  $e$  and  $\mu$  are very close to each other and  $g - 2$  for the  $\tau$  is poorly known
- [45]  $1 \mu b = 10^{-4} \text{ fm}^2$
- [46] The word coherent is also abusive in this respect, since it is associated to a spin-independent potential  $V_C$ , although strictly speaking, the relation (45) is trivially fulfilled.
- [47] there is a minus sign in [28] due to different phase convention.